

COMPARISON OF THE STEADY-STATE AND DYNAMIC PERFORMANCE OF TWO FIXED-GEOMETRY JOURNAL BEARINGS

Martin J. Conlon*, Azzedine Dadouche and Waldemar M. Dmochowski

Gas Turbine Laboratory
National Research Council
Ottawa, Ontario, Canada

ABSTRACT

This paper evaluates two different journal bearings: a cylindrical bore plain journal bearing and a tri-lobe taper land bearing. Each bearing has the same nominal diameter (89 mm) and aspect ratio ($L/D = 0.7$). The shaft rotational speed ranged from 6 krpm to 14 krpm and the bearing specific load from 700 kPa to 2800 kPa.

The bearings' steady-state performance is evaluated according to relative bearing and shaft displacement, bearing operating temperature and power loss. A frequency-domain analysis is used to determine bearing rotordynamic coefficients – it treats the bearing as a mass-spring-damper system. Excitation frequencies range between 20 Hz and 350 Hz.

Ultimately, the tri-lobe taper land bearing offers better stability whereas the cylindrical bore plain journal bearing has a lower eccentricity and runs cooler for a given operating condition. The dynamic properties of the two bearings are found to be similar, although the higher stability of the tri-lobe taper land bearing is also reflected in the dynamic coefficients.

NOMENCLATURE

ρ	Density
σ_u	Standard deviation associated with u
ω	Frequency
A_i	Acceleration, frequency domain
b_{ij}	Damping coefficient
c_p	Specific heat
D	Bearing diameter

F_i	Force, frequency domain
G_{uv}	Power spectral density of arbitrary functions u and v
H_{ij}	Frequency response function
i	Directional index (x corresponds to horizontal direction, y corresponds to vertical)
j	Directional index (x corresponds to horizontal direction, y corresponds to vertical)
k_{ij}	Stiffness coefficient
L	Bearing length
m_u	Mass associated with u
P	Power
Q	Flow rate
S_i	Positional coordinate, frequency domain
T	Temperature
u	Function index (placeholder)
v	Function index (placeholder)

INTRODUCTION

Hydrodynamic bearings are widely used for rotor support in a variety of rotating systems. Rigid geometry bearings have higher load capacity than variable-geometry (tilting-pad) bearings and are suitable for steady-state operating regimes [1], but their oil-film force is the main cause for instability of rotors [2]. Proper design of these bearings is necessary for the successful operation of rotating machinery [3].

Rotordynamic analysis relies on fluid-film bearing force coefficients for prediction of rotor response to imbalance and rotor-bearing stability maps [4]. For rigid geometry journal bearings,

*Address all correspondence to this author.

performance parameters and dynamic force coefficients are understood to be functions of the Sommerfeld number [5].

Over the last few decades, many investigations of multi-lobe bearing designs have been performed and numerical simulations continue to be a focus. Most recently, Rao et al. [6] used a non-linear transient approach to study the stability of a tri-lobe journal bearing under steady, periodic and variable rotating loads. The authors noted that for both the uni-directional and the variable loading cases the bearing reaches a stable position at a faster rate with an increase in ramp size. The bearing was found to be susceptible to instability under the influence of periodic loads.

Rao et al. [7] extended the formulation developed by Reason and Narang [8] to predict the dynamic coefficients of multi-lobe journal bearings using a finite perturbation approach. The results were found to be in agreement with those obtained using a numerical infinitesimal perturbation method at higher eccentricity ratios. In another study, Rao and Sawicki [9] predicted the dynamic coefficients of the same multi-lobe bearings (two-axial groove, elliptical, tri-lobe and offset cylindrical) using a mass conservation algorithm in combination with Jakobsson-Floberg-Olsson (JFO) cavitation boundary conditions. The authors observed that the offset cylindrical bearing had the highest stability threshold at lower eccentricity ratios, as its cross-coupled coefficients were both positive. As eccentricity increased, the elliptical bearing showed better stability.

Ene et al. [10] presented a stability analysis of a three-wave journal bearing, studying the effect of wave amplitude and oil supply pressure on bearing dynamic behavior. They showed (numerically and experimentally) that a bearing with a wave amplitude ratio of 0.305 can run stable up to 60 *krpm* without being affected by sub-synchronous whirl, regardless of the oil supply pressure. Decreasing the wave amplitude ratio to 0.075 produced instabilities and operating speed was then sensitive to oil supply pressure.

Ruiz et al. [11] studied the asynchronous dynamic coefficients of three-lobe air-bearings. The authors observed that the bearing direct stiffness and damping coefficients were frequency dependent while the cross-coupled coefficients were practically null.

This paper presents an experimental evaluation of two different journal bearings performed as part of a bearing development program. Both the plain sleeve bearing and the tri-lobe taper land bearing have the same nominal diameter and the same aspect ratio. The shaft rotational speed ranged from 6 *krpm* to 14 *krpm* (in 2 *krpm* increments) and the bearing specific load from 700 *kPa* to 2800 *kPa* (in 700 *kPa* increments).

Evaluation of the bearings' steady-state performance is based on relative bearing and shaft displacement, bearing operating temperature and power loss. Bearing rotordynamic coefficients are determined using the Power Spectral Density (PSD) method [12].

RIG DESCRIPTION

This study made use of an experimental facility dedicated to measuring the dynamic properties of hydrodynamic bearings. The test rig features a simply-supported, rotating shaft and a free-floating test bearing located at the shaft midspan. A 37 *kW* variable speed electric motor, driving through a belt-and-pulley system provides shaft speeds of up to 16.5 *krpm*. Static load is applied hydraulically through a spring-isolated cable-pulley system and two orthogonal electromagnetic shakers apply dynamic loads to the stator. Each shaker is connected to the bearing housing through a flexure which ensures that the bearing housing is unconstrained in directions perpendicular to the shaking force. Additional detail on the test facility has been previously given elsewhere [13]; a photo is provided in Figure 1.

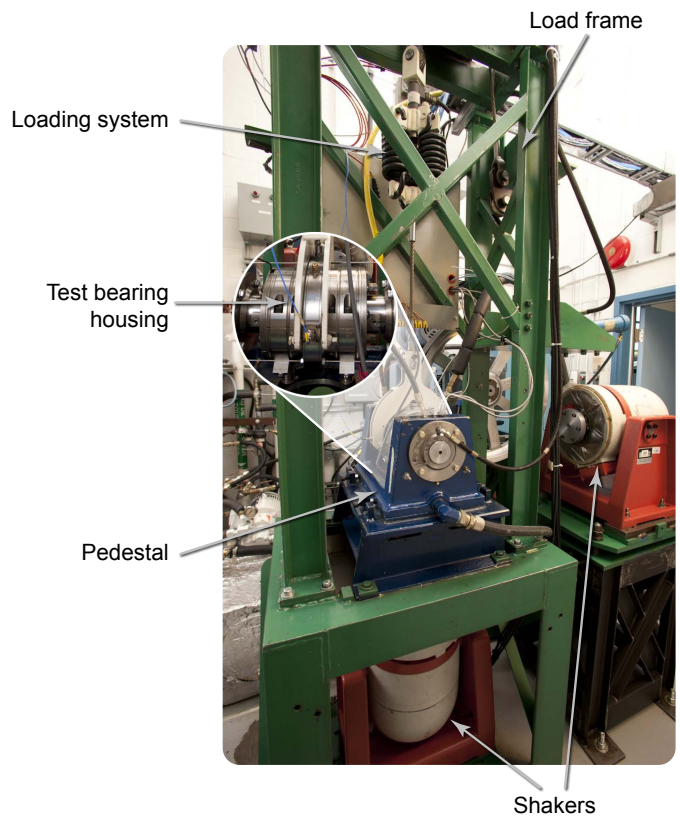


FIGURE 1: Dynamic journal bearing test rig

The bearing housing is instrumented with two single-axis accelerometers (orthogonal to each other) and eight proximity probes (arranged in orthogonal pairs at the axial extents of the bearing housing). Force transducers measure the applied static and dynamic loads.

A 16 bit data acquisition system records the following test bearing parameters at 5.12 kHz:

- Applied static load ($\pm 25 N$)
- Applied dynamic load ($\pm 20 N$)
- Bearing horizontal and vertical position ($\pm 2.54 \mu m$)
- Bearing horizontal and vertical acceleration ($\pm 0.01 g$)
- Shaft rotational speed ($\pm 5 rpm$)
- Bearing temperatures ($\pm 0.5^\circ C$)
- Lubricant inlet and outlet temperatures ($\pm 0.5^\circ C$)
- Lubricant flow rate ($\pm 0.5\%$)
- Lubricant supply pressure ($\pm 500 Pa$)
- Rig power loss ($\pm 100 W$)

Table 1 presents the test rig performance specifications.

TABLE 1: Test rig specifications (performance limits)

Shaft speed (<i>krpm</i>)	0 – 16.5
Journal diameter (<i>mm</i>)	90
Static load (<i>kN</i>)	0 – 22
Dynamic load (<i>kN</i>)	0 – 1.3
Frequency of excitation (<i>Hz</i>)	20 – 7500
Lubricant flow rate (<i>l min⁻¹</i>)	40
Lubricant inlet temperature (<i>°C</i>)	100
Power (<i>kW</i>)	40

BEARING DESCRIPTIONS

The first test bearing is a two axial groove journal bearing with a cylindrical or straight bore. The bearing bore is 89.134 mm and the length is 62.5 mm. The clearance ratio of the bearing is 0.0026. Each axial groove is 52.8 mm long, 1.9 mm deep and covers a 30° arc. The steel bearing is lined with ASTM-B23 Alloy 2 babbitt (white metal) and fitted with 14 Type-T thermocouples, as illustrated in Figure 2.

The second test bearing is a tri-lobe, taper land journal bearing. Each of the three lobes consists of an undercut (taper) extending from the leading edge to the bearing bore (land), which is concentric with the bearing OD. Taper depth and arc angle are designed to satisfy performance requirements. The width of the taper is typically as wide as the axial groove is long. In this particular case, the bearing bore is 89.134 mm and the length is 62.5 mm. The clearance ratio is 0.0026. Each axial groove is 52.8 mm long, 2.4 mm deep and covers a 20° arc; each taper has

TABLE 2: Test bearing specifications

Bearing bore (<i>mm</i>)	{89.134, 89.146}
Bearing length (<i>mm</i>)	{62.36, 62.61}
Clearance ratio ($\times 10^{-3}$)	{2.11, 2.25}
L/D ratio	0.7

a 70° extent. The steel bearing is lined with ASTM-B23 Alloy 2 babbitt and fitted with 14 Type-T thermocouples, as illustrated in Figure 3.

TEST PARAMETERS

For both the steady-state and dynamic testing (and for both bearings) the shaft rotational speed ranged from 6 *krpm* to 14 *krpm* (in 2 *krpm* increments) and the bearing specific load from 700 *kPa* to 2800 *kPa* (in 700 *kPa* increments). Both bearings were found to be unstable at the high-speed, low-load test conditions. As expected, the tri-lobe taper land bearing had better stability than the cylindrical bore plain journal bearing and data was collected at four additional operating conditions. Table 3 presents the complete test matrix — steady-state and dynamic data were collected for all stable operating points at the flow rates

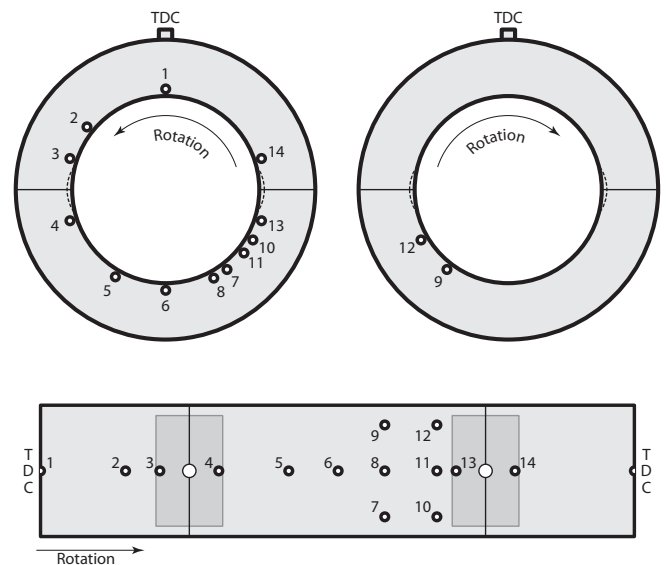


FIGURE 2: Illustration of the cylindrical bore plain journal bearing. Smaller black circles on the planform indicate the thermocouple locations and the shaded gray area shows the extent of the oil feed grooves. Bearing split lines are also indicated.

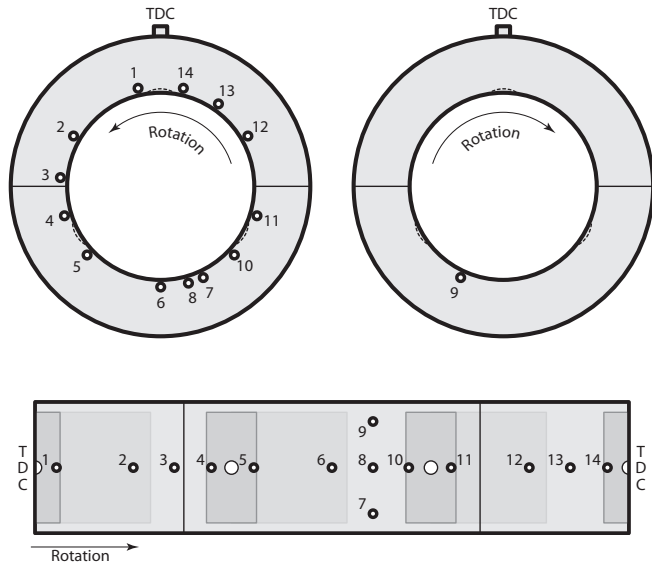


FIGURE 3: Illustration of the tri-lobe taper land bearing. Smaller black circles on the planform indicate the thermocouple locations and the shaded gray areas show the extent of the oil feed grooves and tapers. Bearing split lines are also indicated.

indicated. Both bearings were lubricated by ISO VG 32 turbine oil, with a constant inlet temperature of 49°C .

TABLE 3: Test bearing oil flow rate ($l\text{min}^{-1}$)

Shaft Speed ($krpm$)	Bearing Load (kPa)			
	700	1400	2100	2800
6	6.4	7.1	7.4	7.5
8	8.2 ^a	9.0	9.5	9.8
10	–	10.9 ^a	11.4	11.9
12	–	12.9 ^a	13.5	14.0
14	–	–	15.4 ^a	15.9

^aTaper land bearing only — cylindrical bore bearing unstable.

Measured supply groove pressure varied between 225 kPa and 434 kPa for the cylindrical bore plain journal bearing and between 155 kPa and 245 kPa for the tri-lobe taper land bearing.

EXPERIMENTAL PROCEDURE

Positional Datum Point Determination

Positional measurements are referenced to a datum, taken to be the neutral-load position of the bearing on the shaft — the point at which the bearing centre is aligned with the shaft centre. A datum point must be obtained any time the test rig is started, as the bearing orbit for various speed, load and oil flow conditions is calculated and plotted based on measured displacement from this reference position. Rigid geometry journal bearings run at an off-vertical equilibrium position and therefore the geometric bearing centre was established with zero oil flow rate prior to rig rotation using a lift-and-bump check via the loading systems.

Steady-State Tests

The steady-state test procedure was repeated for all stable test points in the test matrices. Test points for each flow rate and speed condition (combination) were recorded beginning with the lightest load and proceeding to the heaviest load. Once the proper oil flow rate, speed and load were established the bearing temperatures were allowed to stabilize over a 5 min period before data was recorded. Previous investigations using this facility have shown that 5 min is sufficient time for the bearing, journal and cradle to reach thermal equilibrium.

Dynamic Test Procedure

The dynamic testing was done with one stinger configuration at a time. Once either the vertical or horizontal stinger was connected, a low amplitude, 80 Hz sine wave was used to excite the test bearing and verify the stinger assembly. A clean and smooth sine wave signal from the force transducer confirmed proper transducer operation and stinger assembly integrity.

The bearing was then excited using a periodic multi-frequency waveform, hereafter referred to as the “engineered waveform.” The engineered waveform is composed of 34 distinct frequencies, equally spaced between 20 Hz and 350 Hz . The individual frequency components are phase-shifted such that the peak-to-peak amplitude of the waveform is minimized [14] and their amplitude is adjusted proportional to the predicted bearing response, as a linear mass-spring-damper system will respond with lower amplitude oscillations for higher frequencies of excitation, given the same level of driving force.

The amplitude of the engineered waveform is limited by either the total allowable bearing displacement or force transducer capacity and the voltage output of the signal generator was adjusted accordingly.

The dynamic data is acquired in two separate stages: first a steady-state datum point is collected and then the bearing’s dynamic response is measured. The steady-state datum point recorded for each test condition is used as a reference for the dynamic testing in order to minimize the influence of any periodic external disturbances — the load, speed and oil flow rate

are established, and bearing temperatures are allowed to stabilize before this data is recorded.

DATA ANALYSIS AND DISCUSSION

Bearing Eccentricity

Figures 4 and 5 present the journal centre location relative to the bearing clearance for the cylindrical bore plain journal bearing and the tri-lobe taper land bearing (respectively). Comparison of the two figures shows that the cylindrical bore plain journal bearing has a larger minimum film thickness than the tri-lobe taper land bearing for all test conditions. While the eccentricity ratio is greater for the tri-lobe taper land bearing, the overall displacement is more biased towards the load direction — the horizontal excursion is minimized.

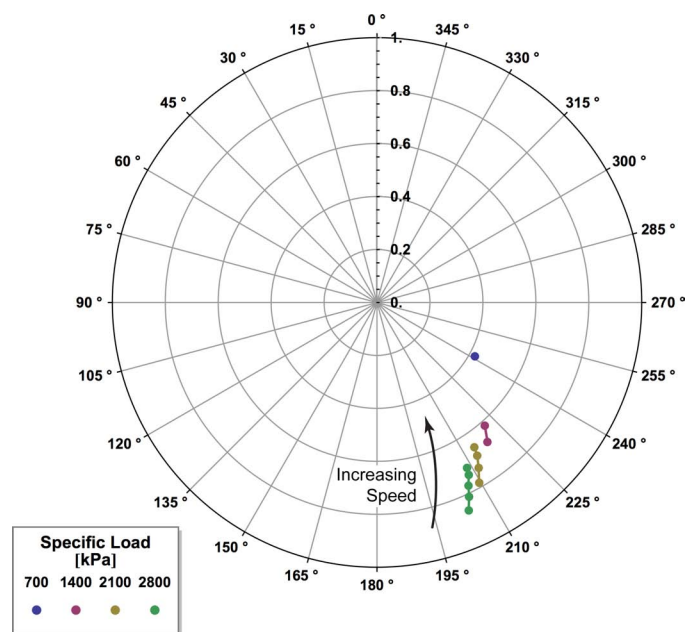


FIGURE 4: Steady-state bearing eccentricity ratio for the cylindrical bore plain journal bearing

Bearing Temperatures

Figures 6(a) through 7(b), which appear at the end of the paper due to their size, present the bearing temperature rise for the highest specific load (2800 kPa) and the highest and lowest speeds (6 krpm and 14 krpm, respectively). This “temperature rise” is the difference between the bearing metal temperature and the oil inlet temperature of 49 °C.

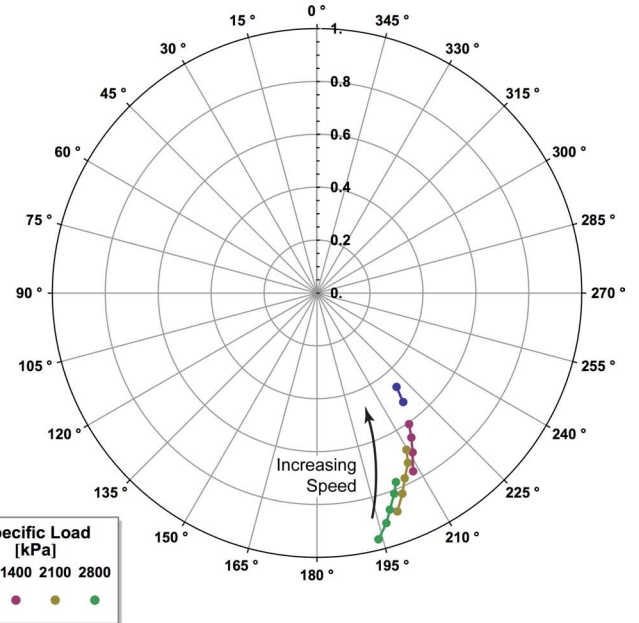


FIGURE 5: Steady-state bearing eccentricity ratio for the tri-lobe taper land bearing

Figure 6(b) indicates that the cylindrical bore plain journal bearing was likely sitting slightly cocked, as the temperature profile is not axially symmetric.

While the temperature profiles for other running conditions are not presented here (in the interests of space), the results show that load has a minor effect on the temperature profile of the cylindrical bore plain journal bearing. Speed, on the other hand has a significant influence, as can be seen by comparing Figures 6(a) and 6(b). The temperature profile of the tri-lobe taper land bearing is affected by both load and speed, the latter having a more significant impact.

The cooling effect of the inlet oil is easily discernable in the bearing temperature profiles, particularly at the higher-speed test conditions, i.e., Figures 6(b) and 7(b). With the tri-lobe taper land bearing the proximity of the oil groove to the loaded area clearly affects the film.

Bearing Power Loss

Figures 8 and 9 present the steady-state power loss for the two bearings. The bearing power loss can be estimated based on the oil inlet and outlet temperatures (ignoring the heat transferred by the oil film into the shaft and housing). The heat balance equation may be written as:

$$P = Q \cdot (T \cdot \rho(T) \cdot c_p(T)) \Big|_{T_{in}}^{T_{out}} \quad (1)$$

where both the specific heat, c_p , and density, ρ , of the oil are functions of temperature.

In addition to this heat balance estimation, the drive motor supply is equipped with a power meter. The data plotted in Figures 8 and 9 are the average of these two power loss values. Due to parasitic losses in the test rig support bearings and in components of the drive system, the power meter readings are always slightly higher (20%, on average) than the estimates obtained using the heat balance. The difference between the two may also be affected by measurement uncertainty of either the power meter ($\pm 100W$) or the heat balance estimation ($\pm 100W$ to $300W$, based on propagation of error for the flowmeter and thermocouples' uncertainties).

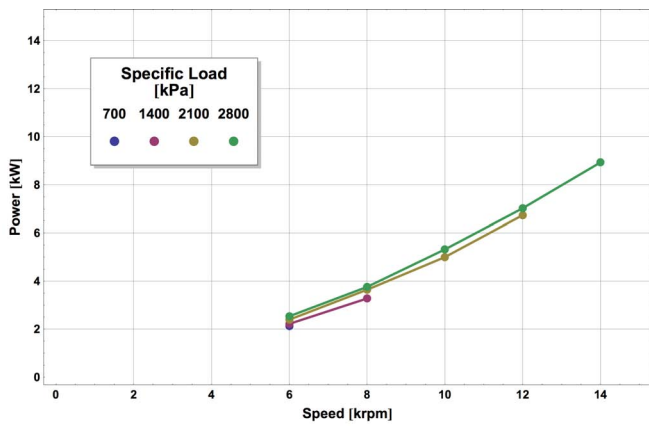


FIGURE 8: Steady-state bearing power loss for the cylindrical bore plain journal bearing

Figures 8 and 9 show that specific load has negligible influence on power loss, while speed has significant influence. This result agrees well with the findings of prior experimental investigations using this test facility, for both tilting-pad and rigid geometry journal bearings, and is supported by the bearing metal temperature data. Comparison of the two bearings shows that the tri-lobe taper land bearing has slightly higher power loss for a given test condition. This finding is also supported by the eccentricity and bearing temperature data wherein the cylindrical bore plain journal bearing had lower eccentricity and a larger minimum film thickness than the tri-lobe taper land bearing.

Bearing Coefficient Determination

The Power Spectral Density (PSD) method [12] was used to determine the stiffness and damping coefficients given the measured excitation forces, bearing displacements and bearing accelerations. The coefficient uncertainty was further evaluated as per Dmochowski and Dmochowski [15]. Conlon et al. [16] presents

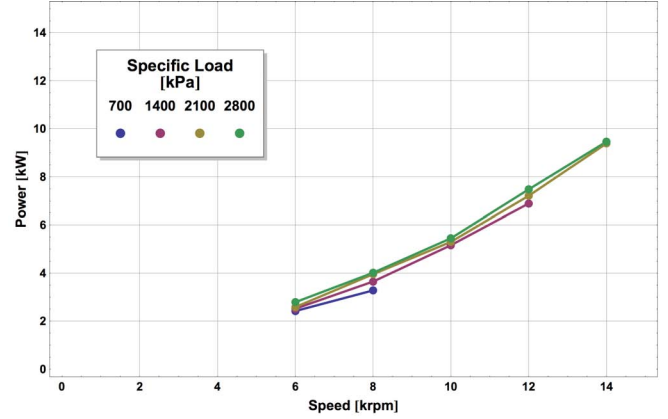


FIGURE 9: Steady-state bearing power loss for the tri-lobe taper land bearing

the basis for the PSD method and the uncertainty determination; the frequency response function (FRF) is reproduced here to facilitate discussion:

$$\begin{bmatrix} H_{xx} & H_{xy} \\ H_{yx} & H_{yy} \end{bmatrix} = \left(\frac{1}{G_{F_x S_x} G_{F_y S_y} - G_{F_x S_y} G_{F_y S_x}} \right) \dots \\ \dots \left(\begin{bmatrix} G_{F_x F_x} & G_{F_y F_x} \\ G_{F_x F_y} & G_{F_y F_y} \end{bmatrix} - m_0 \cdot \begin{bmatrix} G_{F_x A_x} & G_{F_y A_x} \\ G_{F_x A_y} & G_{F_y A_y} \end{bmatrix} \right) \dots \\ \dots \begin{bmatrix} G_{F_y S_y} & -G_{F_y S_x} \\ -G_{F_x S_y} & G_{F_x S_x} \end{bmatrix} \quad (2)$$

Bearing excitation is taken as the input to the system and displacement and acceleration as outputs. This produces four complex frequency response functions from which the bearing stiffness and damping properties can be determined. In order to minimize the effect of any external disturbances and signal noise, the bearing response is ensemble-averaged in the frequency domain. Additionally, the steady-state dynamic data is used to eliminate any DC-offset (by subtracting the mean value) and any external periodic influence (by subtracting the spectrum in the frequency domain). Bearing dynamic properties are then determined from the resultant frequency response functions.

The uncertainty associated with the FRF can be determined by evaluating the propagation of error; we calculate the sensitivity coefficients associated with each measurement. Assuming the uncertainties affecting each signal are uncorrelated, the uncertainty of a particular result is:

$$\sigma_{H_{ij}}^2 = \sum_{k=1}^n \left(\frac{\partial H_{ij}}{\partial u_k} \right)^2 \sigma_{u_k}^2 \quad (3)$$

The PSD method is sensitive to acquisition parameters and system noise, particularly in the higher frequencies where the displacement amplitudes are quite small. The signal power is estimated using Welch's method [17], as follows:

- The 10s signal is partitioned into overlapping windows of length 0.1s (i.e., two periods of the engineered waveform); the overlap is chosen as 0.05s
- A Hann window is applied to each segment in order to minimize leakage and the discrete Fourier transform is computed
- The segments are ensemble-averaged in the frequency domain

Figures 10(a) through 13(d) present the direct and cross-coupled stiffness and damping coefficients for the two bearings.

The two bearings display very similar stiffness and damping. There is a slight difference in the direct stiffnesses (k_{xx} and k_{yy}) — the cylindrical bore plain journal bearing has a slightly higher k_{xx} and the tri-lobe taper land bearing has a slightly higher k_{yy} . This result is anticipated from the bearing eccentricity data, as the cylindrical bore plain journal bearing had a larger horizontal excursion for a given load, whereas the tri-lobe taper land bearing had an excursion that was more biased towards the load direction. The attitude of the cylindrical bore plain journal bearing is therefore more horizontal and the attitude of the tri-lobe taper land bearing more vertical; this orientation affects the film and thus the stiffness. Neither bearing shows a strong frequency dependence, although the plain journal bearing's synchronous coefficients (233.33 Hz, in the plots presented) are substantially different from the non-synchronous coefficients. This reinforces the earlier observation that the tri-lobe taper land bearing has superior stability.

The cross-coupled stiffness coefficients (k_{xy} and k_{yx}) of both bearings, shown in Figures 10(b), 10(c), 12(b) and 12(c), have negative signs indicating that the bearings are dynamically stable. This interpretation is supported by the findings of Rao and Sawicki [9] who showed that offset bearings have a higher stability threshold (compared to other multi-lobe bearings) because their cross-coupled stiffness coefficients have consistent signs. More recently, Ertas and Vance [18] showed that same-sign cross-coupled stiffness coefficients do not generate a destabilizing force in the direction of the whirl velocity. Only the special case where the two cross-coupled stiffness coefficients are of opposite sign is destabilizing.

CONCLUSIONS AND FUTURE WORK

An experimental investigation was performed to determine the steady-state and dynamic characteristics of two different rigid geometry bearings with similar clearance ratios. The main conclusions are as follows:

- The cylindrical bore plain journal bearing has a lower eccen-

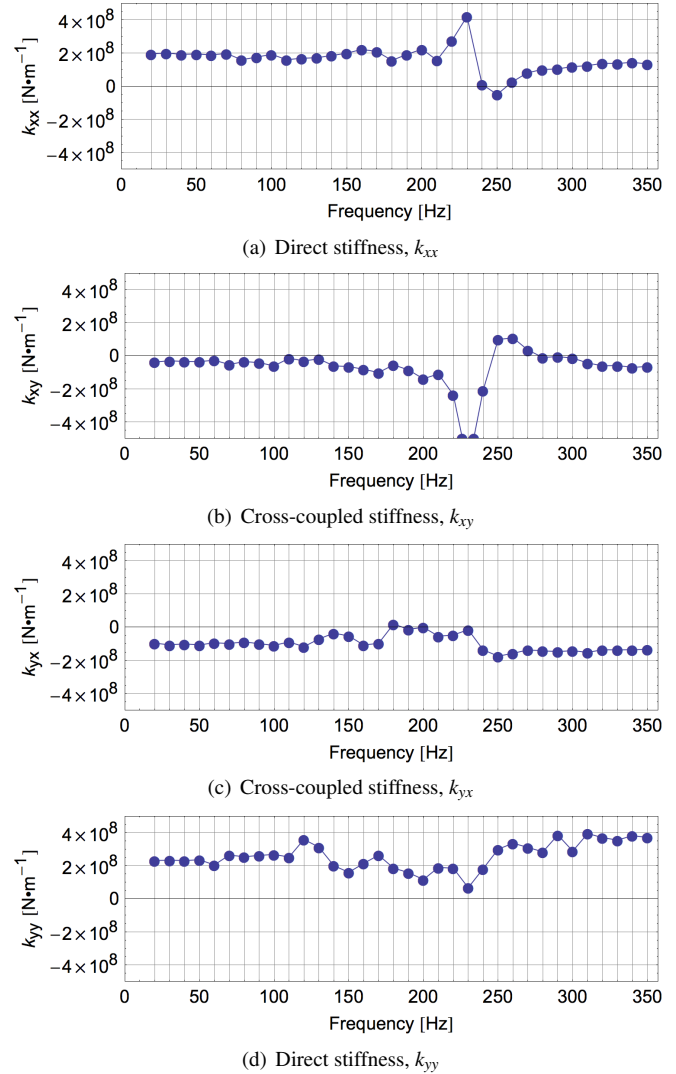


FIGURE 10: Frequency-dependent stiffness coefficients for the cylindrical bore plain journal bearing for a specific load of 2800kPa and a speed of 14krpm

tricity than the tri-lobe taper land bearing for a given load condition.

- The tri-lobe taper land bearing has better stability than the cylindrical bore plain journal bearing for a given specific load.
- The attitude angle of the tri-lobe taper land bearing is more biased towards the load direction, resulting in a slightly higher direct stiffness coefficient, k_{yy} ; the reverse is true for the cylindrical bore plain journal bearing.
- Both bearing metal temperatures are affected by the oil groove locations, with the cooler inlet oil limiting the extent of the heat affected zone.

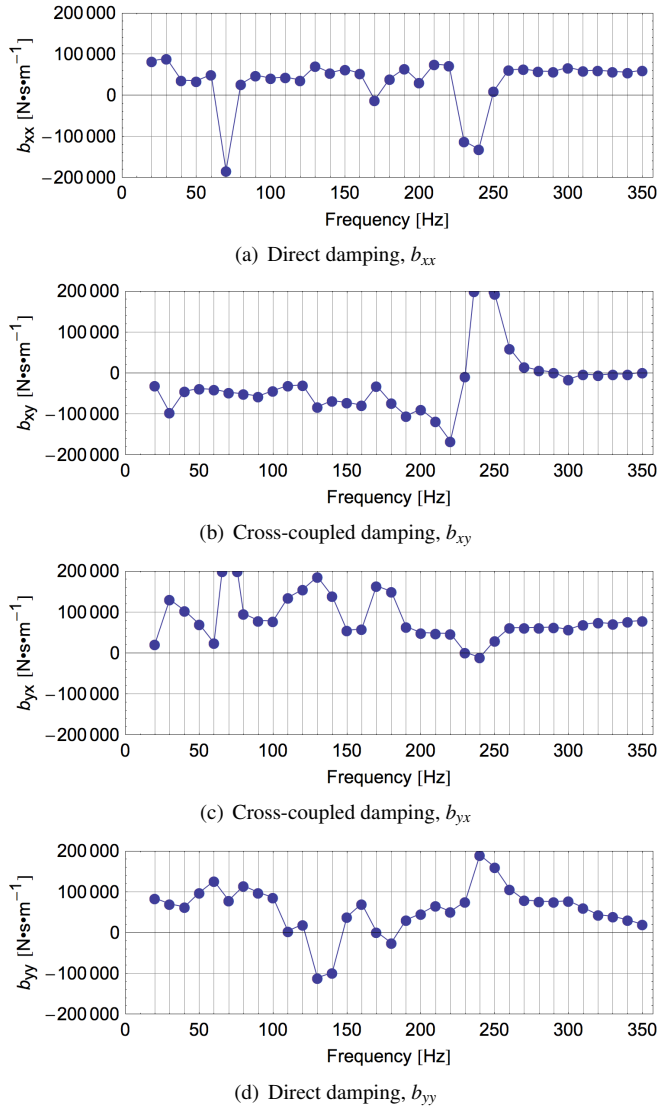


FIGURE 11: Frequency-dependent damping coefficients for the cylindrical bore plain journal bearing for a specific load of 2800kPa and a speed of 14krpm

- Bearing temperatures and power loss are more sensitive to speed than to load.

Future work will include refinement of the dynamic coefficient determination method and investigation of a new asymmetric journal bearing design.

REFERENCES

[1] Brito, F., Miranda, A., Bouyer, J., and Fillon, M., 2007. “Experimental investigation of the influence of supply temperature and supply pressure on the performance of a two-

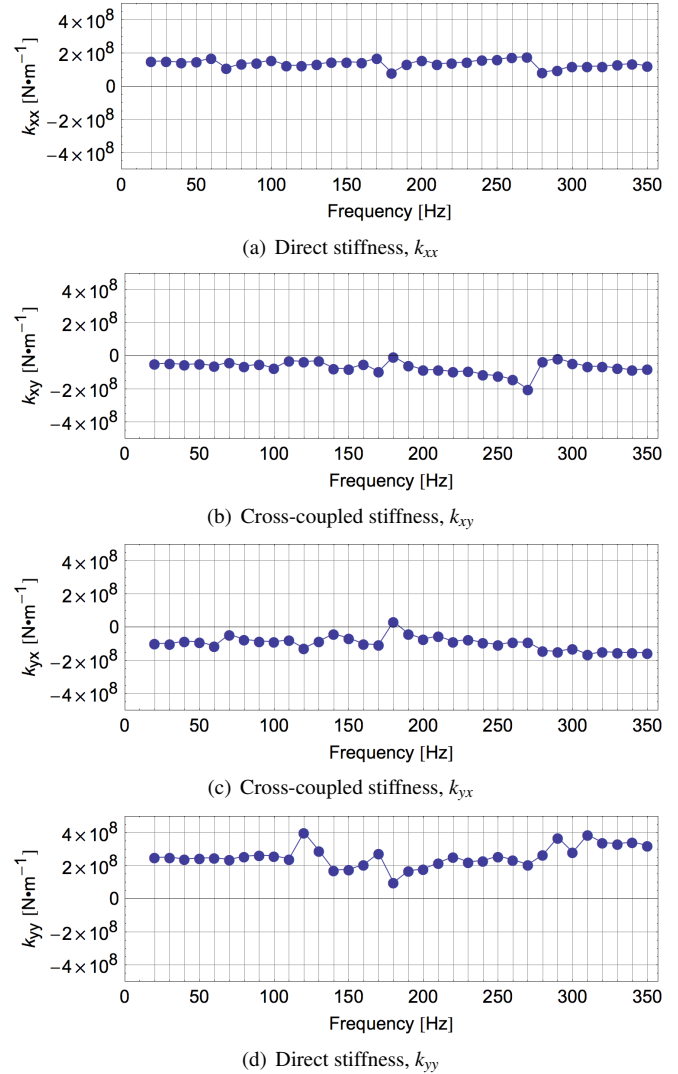


FIGURE 12: Frequency-dependent stiffness coefficients for the tri-lobe taper land bearing for a specific load of 2800kPa and a speed of 14krpm

axial groove hydrodynamic journal bearing”. *J. Tribol.*, **129**(1), pp. 98–105.

[2] Jin Fu, Y., Ce, C., Da Ren, Y., Ying, C., Sheng Bo, Y., Kun, Y., and Zhong Guang, F., 2008. “An analytical model of oil-film force on hydrodynamic journal bearing of finite length”. No. GT2008-50251 in Proceedings of ASME Turbo Expo 2008.

[3] Dimond, T., Sheth, P., Allaire, P., and He, M., 2009. “Identification methods and test results for tilting pad fixed geometry journal bearing dynamic coefficients — a review”. *Shock Vib.*, **16**(1), pp. 13–43.

[4] Sawicki, J., and Rao, T., 2001. “Nonlinear prediction of rotordynamic coefficients for a hydrodynamic journal bear-

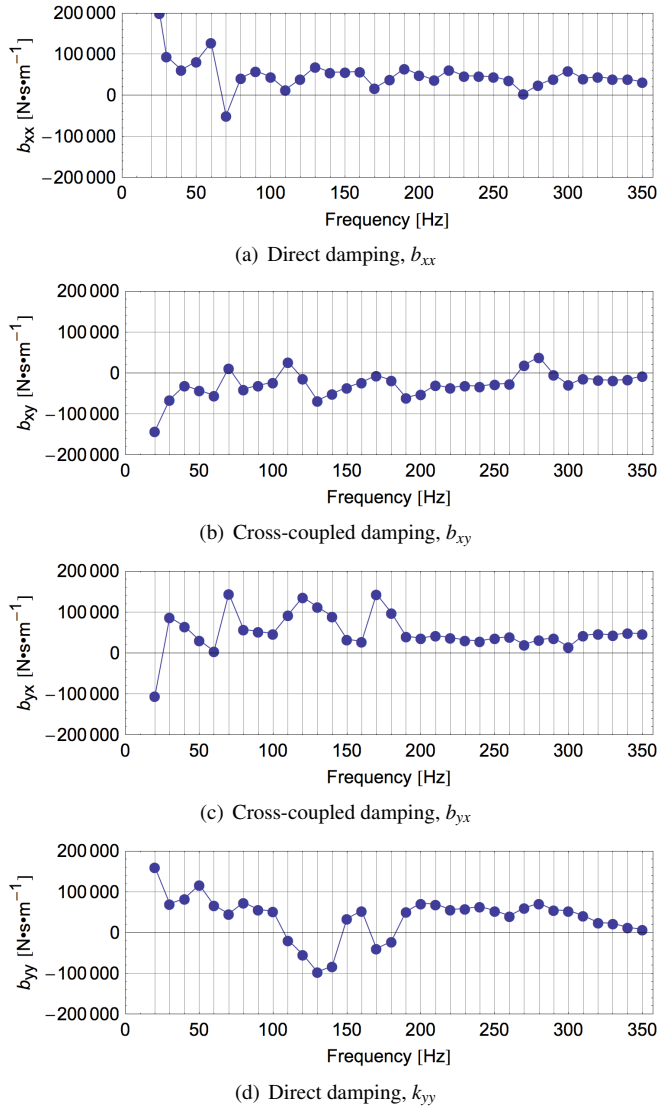


FIGURE 13: Frequency-dependent damping coefficients for the tri-lobe taper land bearing for a specific load of 2800kPa and a speed of 14krpm

ing”. *Tribol. Trans.*, **44**(3), pp. 367–674.

[5] San Andrés, L., and de Santiago, O., 2005. “Identification of journal bearing force coefficients under high dynamic loading centered static operation”. *Tribol. Trans.*, **48**(1), pp. 9–17.

[6] Rao, D., Shenoy, B., Pai, R., and Pai, R., 2010. “Stability of tri-taper journal bearings under dynamic load using a nonlinear transient method”. *Tribol. Int.*, **43**(3), pp. 1584–1591.

[7] Rao, T., Biswas, S., and Athre, K., 2001. “A methodology for dynamic coefficients and nonlinear response of multi-lobe journal bearings”. *Tribol. Trans.*, **44**(1), pp. 111–117.

[8] Reason, B., and Narang, I., 1982. “Rapid design and performance evaluation of steady state journal bearings — a technique amenable to programmable hand calculators”. *ASLE Trans.*, **25**(4), pp. 429–444.

[9] Rao, T., and Sawicki, J., 2003. “Dynamic coefficient prediction in multi-lobe journal bearings using a mass conservation algorithm”. *Tribol. Trans.*, **46**(3), pp. 414–420.

[10] Ene, N., Dimofte, F., and Keith Jr., T., 2008. “A stability analysis for a hydrodynamic three-wave journal bearing”. *Tribol. Int.*, **41**(5), pp. 434–442.

[11] Ruiz, R., Di Liscia, M., Medina, L., and Díaz, S., 2008. “Asynchronous dynamic coefficients of a three-lobe air bearing”. *J. Eng. Gas Turbine Power*, **130**(5), p. 052502.

[12] Rouvas, C., and Childs, D., 1993. “A parameter identification method for the rotordynamic coefficients of a high Reynolds number hydrostatic bearing”. *J. Vib. Acoust.*, **115**(3), July, pp. 264–270.

[13] Dmochowski, W., and Brockwell, K., 1995. “Dynamic testing of tilting-pad journal bearings”. *Tribol. Trans.*, **38**(2), pp. 261–268.

[14] Schroeder, M., 1970. “Synthesis of low-peak-factor signals and binary sequences with low autocorrelation”. *IEEE Trans. Inf. Theory*, **16**(1), January, pp. 85–89.

[15] Dmochowski, W., and Dmochowski, J., 2005. “Frequency dependent dynamic properties of tilting pad journal bearings: experimental results and uncertainty analysis”. No. WTC2005-63274 in Proceedings of the World Tribology Congress III.

[16] Conlon, M., Dadouche, A., Dmochowski, W., Payette, R., Bédard, J.-P., and Liko, B., 2009. “Experimental evaluation of foil bearing performance: steady state and dynamic results”. No. GT2009-60186 in Proceedings of ASME Turbo Expo 2009.

[17] Welch, P., 1967. “The use of fast fourier transform for the estimation of power spectra: a method based on time averaging over short, modified periodogram”. *IEEE Trans. Audio Electroacoust.*, **15**(2), June, pp. 70–73.

[18] Ertas, B., and Vance, J., 2007. “The influence of same-sign cross-coupled stiffness on rotordynamics”. *J. Vib. Acoust.*, **129**(1), February, pp. 24–31.

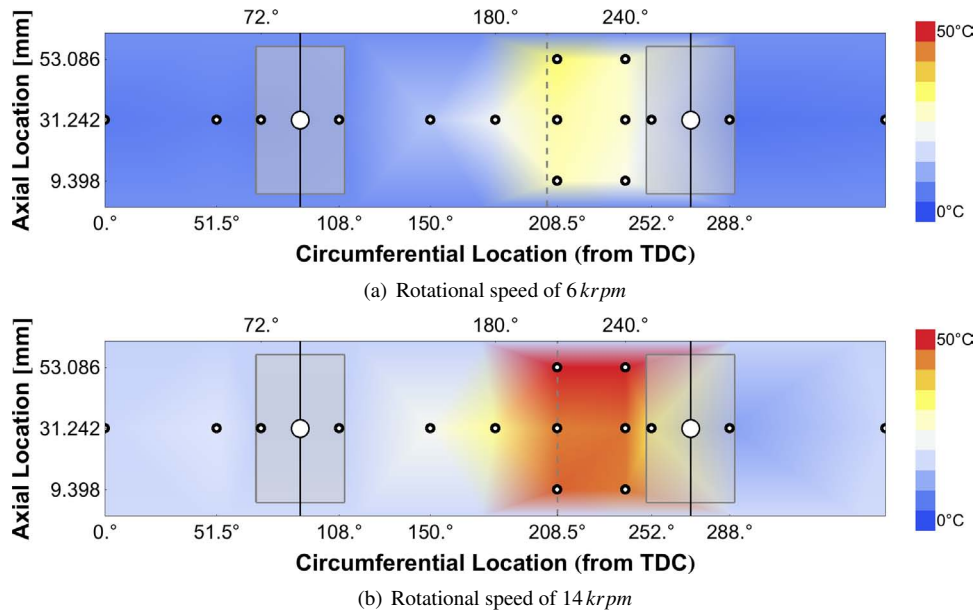


FIGURE 6: Cylindrical bore plain journal bearing temperature rise for a specific load of 2800 *kPa*. Dashed lines show the locations of minimum film thickness. Journal rotation is from left to right.

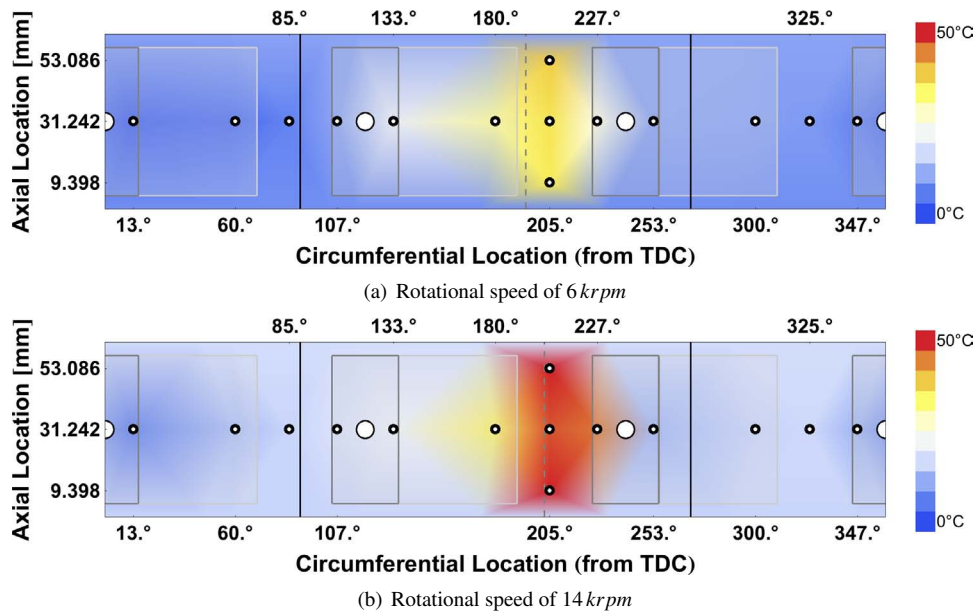


FIGURE 7: Tri-lobe taper land journal bearing temperature rise for a specific load of 2800 *kPa*. Dashed lines show the locations of minimum film thickness. Journal rotation is from left to right.